Currents and shear Alfvén wave radiation generated by an exploding laser-produced plasma: Perpendicular incidence

M. VanZeeland,[a] W. Gekelman, S. Vincena, and J. Maggs
Department of Physics and Astronomy, University of California, Los Angeles, California 90095-1547

(Received 6 November 2002; accepted 7 February 2003)

Examples of one plasma expanding into another and the consequent radiation of wave energy are abundant in both nature and the laboratory. This work is an experimental study of the expansion of a dense laser-produced plasma (initially, $n_{lpp}/n_0 \gg 1$) into a magnetized background plasma ($n_0 = 2\times10^{12}$ cm^{-3}) capable of supporting Alfvén waves. The experiments are carried out on the upgraded Large Plasma Device (LAPD) at UCLA [W. Gekelman *et al.*, Rev. Sci. Instrum. **62**, 2875 (1991)]. It has been observed that the presence of a background plasma allows laser-plasma charge separation to occur that would otherwise be limited by large ambipolar fields. This charge separation results in the creation of current structures which radiate shear Alfvén waves. The waves propagate away from the target and are observed to become plasma column resonances. Conditions for increased current amplitude and wave coupling are investigated. © *2003 American Institute of Physics.* [DOI: 10.1063/1.1564598]

I. INTRODUCTION

The basic physics of a spatially localized plasma expanding and moving into an ambient plasma and the consequent radiation of wave energy is fundamental in many areas of astronomy and plasma physics. Astrophysical explosions, irrespective of scale, are responsible for enormous releases of energy and plasma into the surrounding ionized media. Coronal mass ejections (CME)[1] may play a key role in the dynamics of space weather and the origin of turbulence in the solar wind. Additionally, CME's have been observed to be associated with outward propagating Alfvén waves.[2] In laboratory fusion experiments, tokamak pellet injection severely impacts the background plasma, radiates waves, and sometimes causes disruptions.[3,4] In the Earth's ionosphere, the 1962 detonation of a 1.5 Megaton nuclear device at an altitude of 400 km (project STARFISH) is believed to have radiated Alfvén waves which later turned into standing modes on the Earth's field lines.[5] Also in the ionosphere, the Active Magnetospheric Particle Tracer Explorers (AMPTE) and Combined Release and Radiation Effects Satellite (CRRES) barium release experiments created another example of high density plasma interacting with a dilute background plasma.[6,7]

As early as 1964 it was recognized that a laser delivering power densities above 10^{10} W/cm^2 could efficiently produce hot plasmas with the bulk of the laser energy mainly deposited into ion kinetic energy.[8] Since then, major advances in laser technology have created a growing area of research utilizing laser-produced plasmas (lpp) for a broad range of fields, including fusion research,[9–11] simulation of exploding supernovae[12,13] and thin film deposition.[14] The experiment presented here centers on the use of a laser to generate rapidly expanding, dense plasmas embedded in a background plasma.

A laser-produced plasma exploding into an ambient magnetized plasma with our parameters, triggers a variety of phenomena which span several orders of magnitude in space and time. For instance, in the first several nanoseconds after impact, x rays and other electromagnetic radiation are emitted and some atoms in the vicinity of the target are photoionized. Also, on this time scale Langmuir waves and fast electrons (<100 eV) emanate from the target region. On the order of microseconds a diamagnetic cavity forms and the bulk laser-produced plasma hits its maximum radius while simultaneously generating lower hybrid and Alfvén waves. After 10 to 1000 microseconds, acoustic waves and shocks are formed. This paper is an investigation of the reproducible current structures and shear Alfvén wave radiation that form in the time period between 1/10 and 100 microseconds when a rapidly expanding ($v_{\text{expan}}/v_{\text{Alfvén}} \simeq 0.1-1$), high density ($n_{\text{lpp}} \gg n_0$) laser-produced plasma is embedded in an ambient, steady state, fully magnetized plasma. It is organized as follows: the experimental setup and instruments are described in Sec. II, the experimental results are presented in Sec. III sorted according to direction of expansion and induced currents, together with a discussion of the generated shear Alfvén waves, and Sec. IV presents conclusions.

II. EXPERIMENTAL APPARATUS

The measurements reported in this paper were taken on the upgraded Large Plasma Device (LAPD).[15] The upgraded LAPD is 20 m long and the plasma column length is 17 m. The plasma is formed with a dc discharge. The discharge current ($I_{\text{dis}} \leqslant 15$ kA) emanates from a 80 cm diameter oxide-coated cathode capable of producing quiescent plasmas ($\delta n/n \approx 0.01$) with densities $< 5\times10^{12}$ cm^{-3}, ion temperatures <2 eV, and electron temperatures <10 eV. The background plasma in this experiment was neon $M_i = 20$, $n_o = 2$

[a]Electronic mail: mav@physics.ucla.edu

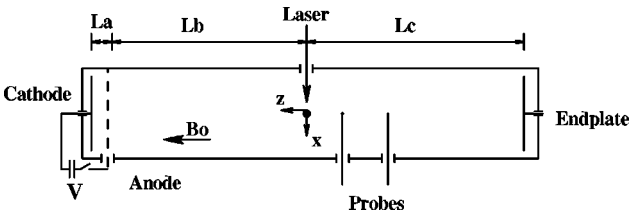

FIG. 1. A schematic of the experimental configuration. La=50 cm, Lb=667 cm, Lc=1033 cm, plasma diameter=50 cm, $B_o=1.5$ kG, $V=50$ V. Magnetic fluctuation data were obtained on perpendicular xy planes 25 cm × 20 cm with $\Delta x=\Delta y=0.5$ cm centered at $x=-7.5$ cm, $y=0$ cm and $z=-2, -34, -130, -194$ cm. The parallel xz planes were 25 cm×12 cm and 25 cm ×24 cm with $\Delta x=0.5$ cm, $\Delta z=1$ cm centered at $x=-7.5$ cm, $y=0$ cm, $z=-6$, and $x=-7.5$ cm, $y=0$ cm, $z=-34$ cm, respectively. Ion-saturation data were obtained on the same size perpendicular planes centered at $x=-7.5$ cm, $y=0$ cm and $z=-34, -130, -354$, and -578 cm. The laser impacts the target surface at $x=0$, $y=0$, $z=0$.

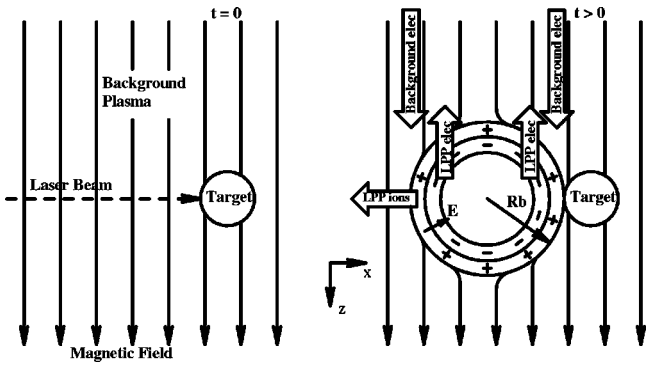

FIG. 2. Simple cartoon of initial laser-plasma expansion into a background plasma. The entire space is filled with a background Ne plasma. Left panel, laser is fired across the background field. Right panel, lpp expands outward with unmagnetized ions dragging electrons across the field. Simultaneously electrons are escaping down field lines (escaping current) and being replaced by background electrons (return current). Cross field neutralization is then accomplished by background ions via polarization drift or electron–ion collisions. R_b is the magnetic bubble radius ≈3.5 cm and E is an ambipolar electric field.

×10^{12} cm^{-3}, $T_e=5$ eV, $T_i=1$ eV, diameter=50 cm as determined by Langmuir probe measurements in a plane. The background magnetic field (B_o) was 1.5 kG and axially uniform. The laser used was a 1.5 J/pulse, 8 ns full width at half-maximum (FWHM), Q-switched Nd-Yag Quanta Ray Pro from Spectra Physics. The extremely repeatable beam is focussed to an on-target spot diameter of 0.5 mm and is both temporally and spatially Gaussian shaped. The target, located 661.5 cm from the cathode, is a 1.9 cm diameter aluminum rod (unless mentioned otherwise) which, to ensure a fresh target surface, is translated and/or rotated using a dual stepper motor system by 1 mm after every five shots. A diagram of the setup is shown in Fig. 1. The coordinate system used is centered at the laser impact point and is also shown in Fig. 1.

The probes used in this experiment are a 3-axis inductive pickup loop system and a Langmuir probe drawing ion saturation current. Each axis of the magnetic probe consisted of a pair of 3-turn loops differentially wound to reduce electrostatic pickup. The total combined area of all six coils for each axis is 0.835 cm^2. The Langmuir probe is planar and has an area of 1 mm^2.

The experiment proceeds as follows: (1) The probe is positioned at some point on a predetermined data acquisition plane using a computer controlled stepper motor system,[16] (2) plasma is pulsed on and allowed to reach a steady state, (3) 0.5 μs before the laser is fired data acquisition begins and continues for 0.32 ms, (4) laser fires, (5) steps 2–4 are repeated for five shots at 1 Hz, (6) target is rotated and/or translated, (7) entire process is repeated at a new probe location.

Data are acquired using a VXI crate and up to four fast Tektronix TVS-645 waveform digitizers (< 4 G samples/s, 8-bit). Several planes of fluctuating magnetic field and ion-saturation data were acquired both perpendicular and parallel to the background field. The received time series of magnetic field and ion-saturation fluctuations were observed to be phase locked from shot to shot so a five-shot ensemble average was used to reduce background noise.

III. EXPERIMENTAL RESULTS

A. Initial perpendicular expansion

When a laser-produced plasma expands across a background magnetic field in vacuum it goes through several phases. The initial laser impact results in immediate ionization of surface atoms and a blast of fast electrons ($E<100$ eV) which rip ions from the target surface due to a large ambipolar field. The more massive ions hold back the electrons and eventually overshoot them due to their relative unmagnetized state. This creates a radially inward directed ambipolar field which in turn causes an electron $\vec{E}\times\vec{B}$ drift and, in conjunction with $\vec{\nabla}P\times\vec{B}$ currents, the observed laser-plasma diamagnetism.[17] When a background plasma is present, this effect is complicated because the background electrons can shuttle along field lines and partially short out the initial large ambipolar field allowing laser-plasma electrons to escape. A schematic of this early-time situation is shown in Fig. 2.[18] The lpp diamagnetic cavity size can be approximated by setting the total excluded magnetic energy equal to the kinetic energy of the laser plasma, E_{lpp}. Namely, a magnetic confinement or ''bubble'' radius $R_b=(3\mu_o E_{lpp}/\pi B_0^2)^{1/3}$,[19–21] where E_{lpp} is approximated as 1/2 the initial laser beam energy, $E_{\mathrm{lpp}}=0.75$ J. Also, the volume has been corrected for expansion into 2π steradians giving $R_b=3.5$ cm for our conditions. Faraday cup measurements in vacuum have shown approximately 2.5×10^{15} particles are ablated with an average perpendicular expansion speed of $v_\perp=1.4\times10^7$ cm/s which corresponds to a kinetic energy about half E_{lpp}. These numbers are consistent with experimentally derived scaling laws and previous experiments citing laser to plasma-kinetic-energy conversion efficiencies as large as 90% at these laser fluences.[22–24] For our typical background densities of 2×10^{12} cm^{-3}, this means that when the lpp has reached the bubble radius it is a factor of approximately 13 more dense than the background plasma. Both the diamagnetic bubble scaling and ambipolar field have been observed in previous experiments where the ex-

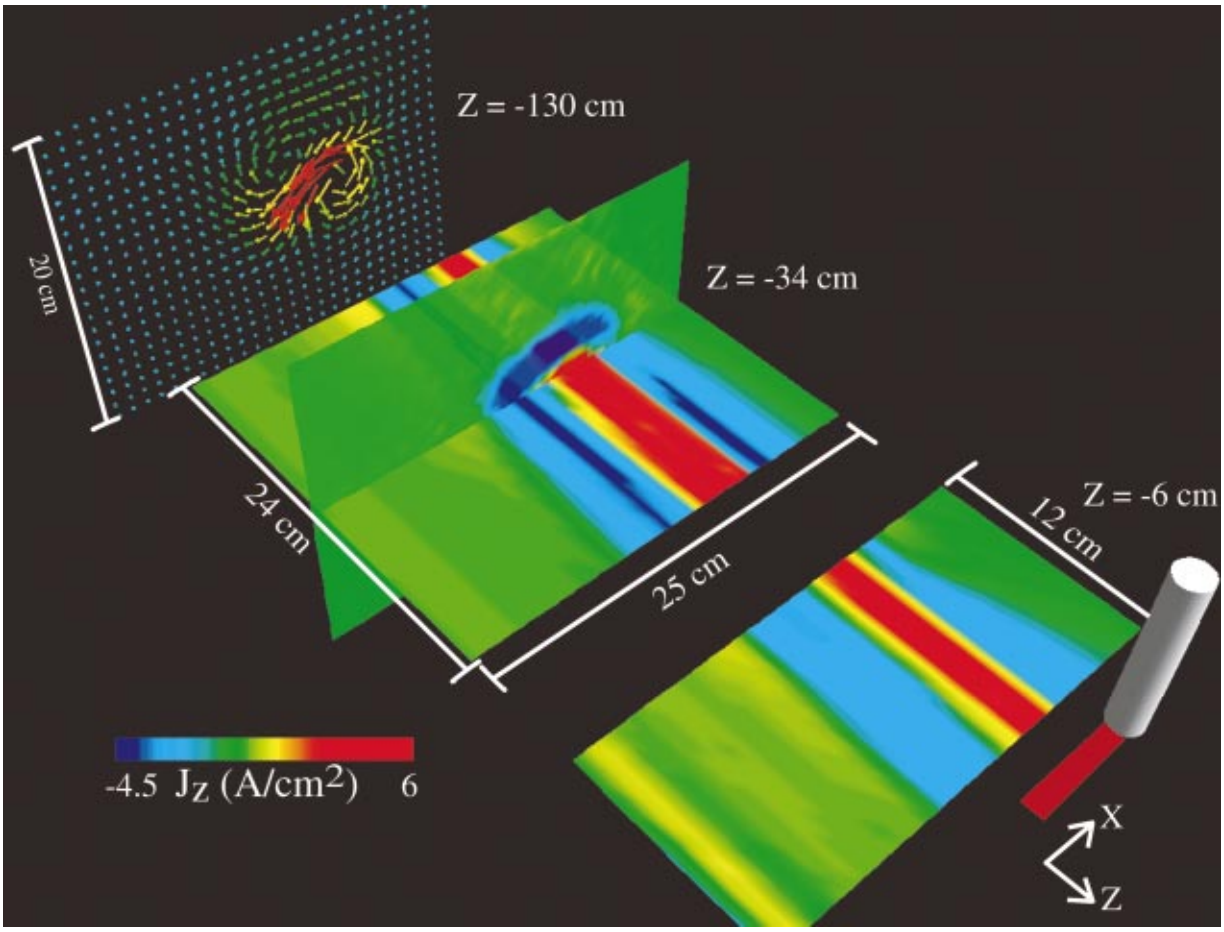

FIG. 3. (Color) Magnetic field data at $t=0.39$ μs. Solid planes are current density obtained from $J=(1/\mu_o)\vec{\nabla}\times\vec{B}$. Red/blue represents electrons going in the $-z/+z$ direction. Vector plot shows perpendicular magnetic field. The target is shown to scale at its approximate location relative to the $z=-6$ cm plane. The red strip near the target indicates the x-direction extent of the diamagnetic cavity. The laser is incident along the x axis. $J_{te}=32$ A/cm^2.

pansion occurred into vacuum[19] and background gas.[20,21,25] They have also been studied by this group for expansion into a background plasma and will be the subject of a future paper.

An example of the initial 3D current structure, derived from measurements of magnetic field and $\vec{J}=(1/\mu_o)\vec{\nabla}\times\vec{B}$, due to escaping electrons and background electron return currents is shown in Fig. 3. In the solid colored planes, red represents positive current density and blue represents negative current density (i.e., electrons going in the negative-z and positive-z direction, respectively). As one might expect, for times less than that of peak diamagnetism, the current distribution is approximately coaxial in nature with the central current channel corresponding to electrons coming from the target plasma and the outer channel associated with electrons from the background plasma. An approximation to this time is given by $\tau_d=2R_b/v_\perp\simeq 0.5$ μs. The plane located at $z=-130$ cm is a vector plot of the fluctuating magnetic field—red indicating higher field values, clearly showing the azimuthal field induced in the background plasma. The red strip next to the cylindrical target is for reference as to the extent and location of the diamagnetic cavity in the x direction.

In order to investigate the effect of background plasma parameters on the outgoing electron current channel, a series of magnetic field data were taken along a line at $z=-34$ cm, $y=0$ cm. The background density and electron temperature were varied by firing the laser at different times after the dc discharge was terminated. Figure 4 shows the temporal dependence of these parameters after shutoff. The e-folding time of the electron temperature is roughly 1 ms and that of the density is 10 ms. The current channel formation takes <1 μs therefore the background plasma parameters are assumed constant over this time. A scaled parameter of relevance to these experiments which incorporates both the changing background density and temperature is the ratio of electron thermal speed to Alfvén speed

$$v_{te}/v_{\text{Alfvén}}=\left(\frac{2kT_e}{m_e}\Big/\frac{B^2}{\mu_o n_o M_i}\right)^{1/2},$$

or alternatively the plasma beta, $\beta=nkT_e/(B^2/2\mu_o)$. The specific temperatures and densities change as to vary $v_{te}/v_{\text{Alfvén}}$ from roughly 2.0 to 0.2.

The resulting return and escaping electron current densities scaled to the background thermal current density ($J_{te}=n_o e v_{te}$) are shown in Fig. 5 for a range of $v_{te}/v_{\text{Alfvén}}$. Parallel current density was calculated from $J_z=(1/\mu_o)\partial_x B_y$ along the line $y=0$. This assumes that

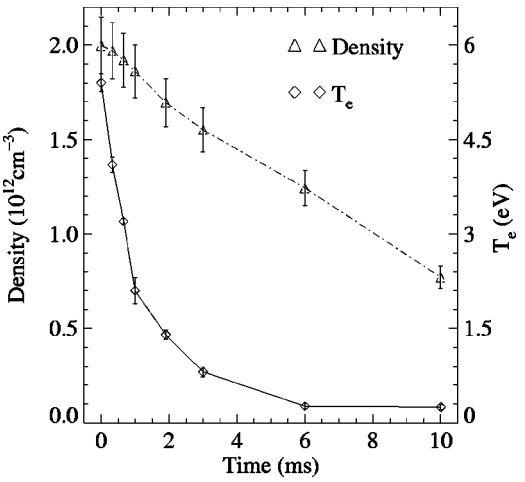

FIG. 4. Background plasma parameters after the discharge current is terminated (termination occurs at $t=0$). This is the afterglow phase. ◇ =electron temperature, △ =plasma density.

$(1/\mu_o)\partial_y B_x = 0$ along this line, which is true for our nearly azimuthally symmetric axial current distributions. This assumption has been verified where B_x and B_y were measured in a plane so that $(1/\mu_o)\partial_y B_x$ could also be computed. For this case, it was found that the error in the magnitude of J_z introduced by neglecting the y derivative of B_x was less than 10% for times earlier than $t=\tau_d$. The same method was used to derive J_z in the parallel planes shown in Fig. 3.

From Fig. 5 we see that for decreasing $v_{te}/v_{\text{Alfvén}}$ the escaping and return currents become a greater fraction of the background thermal current. Specifically, this relation can be approximated by $J = C_o J_{te}(v_{te}/v_{\text{Alfvén}})^{C_1}$ where, using a nonlinear regression fitting routine, C_o and C_1 were determined to be $C_{oe} = 0.3 \pm 0.01$, $C_{1e} = -0.62 \pm 0.04$ and $C_{or} = 0.16 \pm 0.01$, $C_{1r} = -0.68 \pm 0.04$ for the escaping and return current densities respectively. These fits are shown in Fig. 5

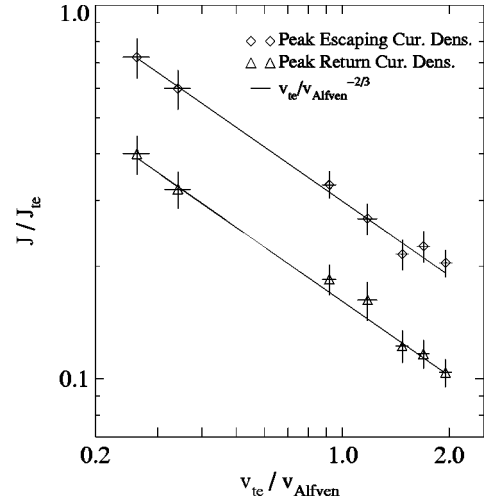

FIG. 5. Peak escaping and return current density normalized to background thermal current (J_{te}) for $y=0$, $z=-34$ cm. Solid line is nonlinear regression fit. $v_{te}/v_{\text{Alfvén}}$ is for the background neon plasma and is varied by firing the laser at different times during the afterglow phase. J_{te} values are 31.1, 26.7, 23.0, 18.0, 13.5, 9.4, 4.3, 2.6 A/cm^2 and correspond to the points in the direction of decreasing $v_{te}/v_{\text{Alfvén}}$.

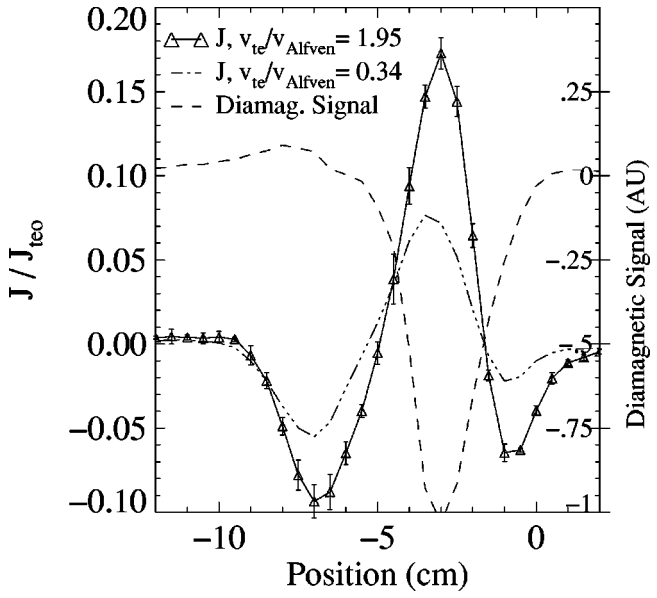

FIG. 6. Solid line is the current density normalized to J_{teo} along a line in the x direction with $y=0$, $z=-34$ cm, $t=0.36$ μs, and $v_{te}/v_{\text{Alfvén}}=1.95$. $J_{teo}=31.1$ A/cm^2 and is the thermal current in background plasma before turnoff. Error bars are shown at each data point location. Dashed–dotted line is the current density normalized to J_{teo} along a line with $y=0$, $z=-34$ cm, $t=0.36$ μs, and $v_{te}/v_{\text{Alfvén}}=0.34$. Dashed line is the diamagnetic cavity as measured along a line in the x direction with $y=0, z=-2$ cm, same time. Skin depth is 0.37 cm for $n_o = 2\times10^{12}$ 1/cm^3.

as solid lines where both C_1 values have been set to $-2/3$. Currently, this dependence is not understood. Not shown in Fig. 5 is that when the experiment was carried out for expansion into vacuum no current channel was detectable. This indicates that there is a value of $v_{te}/v_{\text{Alfvén}}$ when J/J_{te} should go to zero.

Figure 6 shows the current density along $y=0$ cm $z=-34$ cm when the target is struck during the discharge as well as 6 ms after turnoff ($v_{te}/v_{\text{Alfvén}}=1.95$ and 0.34, respectively), overlayed with the diamagnetic field generated near the target by the expansion. The peak positive current density occurs at approximately the cavity center and the return current occurs at the edge of the bubble—consistent with Fig. 2. Two different current density lines were shown to illustrate the fact that the width of the current channel does not change with $v_{te}/v_{\text{Alfvén}}$ and that the absolute magnitude of the currents go down (each signal was normalized to the thermal current before shutoff, $J_{teo}=32$ A/cm^2). The peak return current has been observed to occur when the time rate of change of the escaping current channel is maximum. This indicates that the return current has a significant contribution from the inductive parallel electric field generated by the escaping ballistic lpp electrons. A phenomenon which has been observed in recent particle-in-cell simulations for a supersonic plume moving along a magnetized plasma.[26]

B. Further perpendicular expansion

As the unmagnetized laser-plasma ions continue to expand across the confining magnetic field, dragging electrons along with them, the parallel electron current system induced in the background plasma becomes highly asymmetric. It

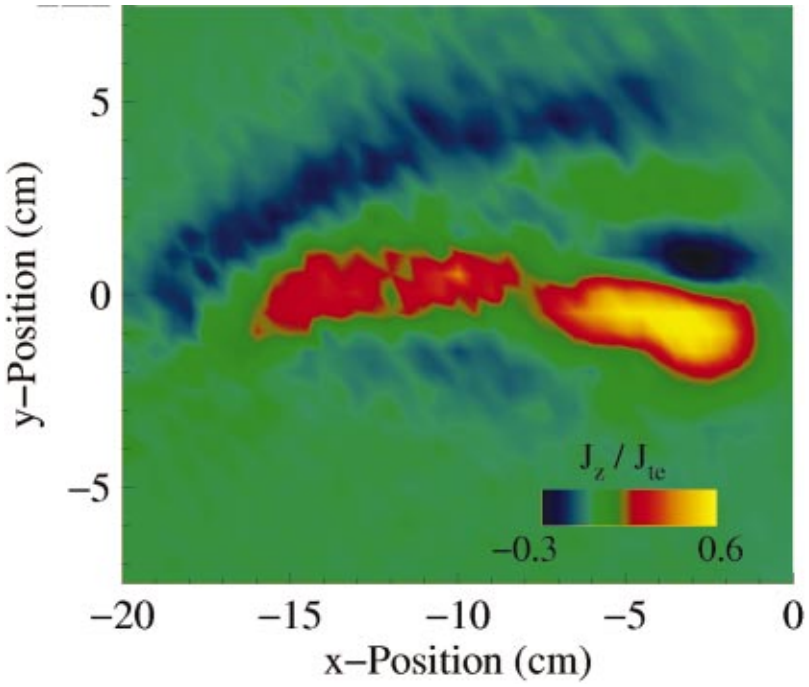

FIG. 7. (Color) Current density as derived from $\vec{J}=(1/\mu_o)\vec{\nabla}\times\vec{B}$ at $z=-34$ cm, $t=1.45$ μs normalized to the background thermal current. Blue represents background electrons going toward lpp ions. Yellow represents background and lpp electrons going away from the lpp. The bulk lpp has not yet arrived at this plane. B_0 points out of the page.

evolves rapidly from a pseudocoaxial system ($t>\tau_d$) to two antiparallel current sheets. At all times, however, the net current through any *x-y* plane has been measured to be zero within experimental error. The axial component of the current density (J_z) at $z=-34$ cm and $t=1.45$ μs is shown in Fig. 7. These data were derived using the measurements taken in a plane where the full $\vec{J}=(1/\mu_o)\vec{\nabla}\times\vec{B}$ could be calculated for J_z and no assumptions about coaxial symmetry were necessary so the late time signals could be investigated. Along with some remnants of the original coaxial structure, two current sheets are clearly visible with the blue/yellow–red representing electrons moving toward/away from the lpp.

This effect can be understood by examination of the charge distribution in the perpendicularly expanding lpp. Mostovych, Ripin, and Stamper examined transverse expansion from a flat surface into a vacuum and consequent jet collimation.[27] The same phenomena occurs here. They suggested that the expanding lpp becomes polarized due to the $\vec{v}\times\vec{B}$ Lorentz force pushing ions to one side and electrons toward the other ($+\hat{y}$ and $-\hat{y}$, respectively). The polarization then produces an electric field which causes the entire plasma to $\vec{E}\times\vec{B}$ drift across the background magnetic field.[28,29] As the lpp continues to expand further, focussing occurs due to curvature of the polarization electric field resulting in a wedgelike jet. Further expansion of the unmagnetized ions allows them to accumulate ahead of the electrons and another electric field forms with its own $\vec{E}\times\vec{B}$ drift in the direction of electron gyromotion ($-\hat{y}$). Our data suggest that this model is correct. Figure 7 shows antiparallel sheetlike electron currents consistent with background and lpp electrons rearranging themselves to compensate for a polarized wedgelike lpp. Additionally, these currents track the curvature of the lpp in the direction of electron gyromotion as can be seen by the curved appearance of the induced sheet currents. The current sheets shown in Fig. 7 are reminiscent of the Alfvén wings or conduction wings discussed by Borovsky.[28] Estimates of the total current based on his results, however, are too large.

Shown in Fig. 8 is the time evolution of the current density observed at four different axial locations at the same perpendicular location. The $x-y$ location was chosen to correspond to that of the peak current observed anywhere in the plane and was found to occur at $x=-3.5$ cm, $y=-1.0$ cm. The signal for $z=-2$ cm is possibly misleading. Although it is normalized to the ambient background thermal current, the thermal current at $z=-2$ cm is probably higher due to x ray and fast electron multiple ionization of the background gas.

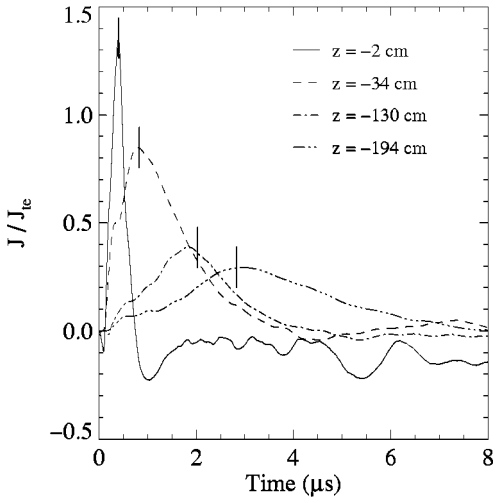

FIG. 8. Largest observed current densities normalized to the background thermal current at four different axial locations, $x=-3.5$ cm, $y=-1$ cm. Solid lines located at the peak of each time series indicate constant propagation speed of 8×10^7 cm/s.

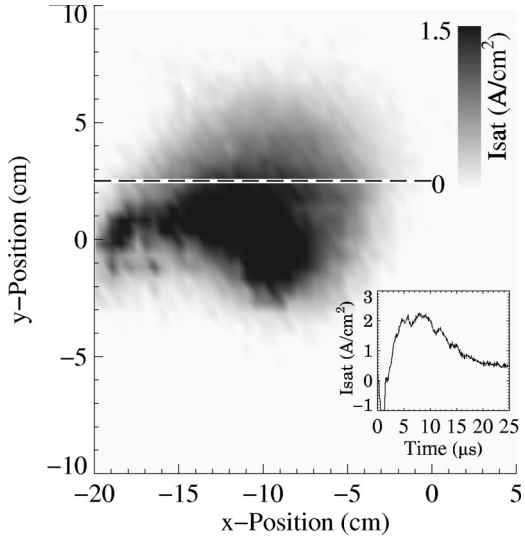

FIG. 9. Ion-saturation current measurement at $z=-34$ cm, $t=4.93$ μs. Inset, time evolved trace at $x=-9.5$ cm, $y=-0.5$ cm. Probe area is 1 mm^2. Dashed line is where time-of-flight data were taken for Fig. 10.

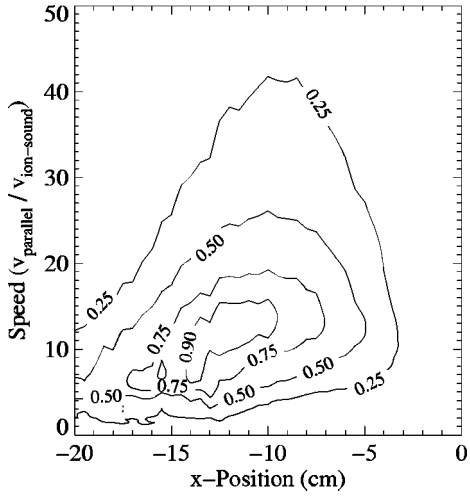

FIG. 10. Contours of relative number of particles with time-of-flight derived speed as a function of x location, $y=2.5$ cm, $z=-34$ cm. Position corresponds to dashed line in Fig. 9. The laser impacts the target at $x=0$. Speed is normalized to ion-sound speed in the background plasma. (Note in the background plasma $v_{te}=10^8$ cm/s, $v_{\text{Alfvén}}=5\times10^7$ cm/s, and $c_s=5\times10^5$ cm/s.)

The solid vertical lines are spaced according to a constant propagation speed of 8.0×10^7 cm/s and nearly coincide with the time of arrival of the peak current at each axial position. This number is larger than the Alfvén speed, but it corresponds to the low frequency limit of the kinetic shear Alfvén wave group and phase speed for a perpendicular wavelength equal to the bubble radius. It is possible that while the escaping electron beam creates a current channel very rapidly, the bulk current propagation speed is being limited by cross-field polarization currents through an Alfvén wave front as predicted by Borovsky.[28] Alfvén wave radiation will be discussed in detail in Sec. III D.

C. Parallel expansion

While expanding in the perpendicular direction, the lpp simultaneously expands along the magnetic field. The parallel component of expansion has a distribution of speeds centered around a value less than the peak perpendicular speed. Shown in Fig. 9 is a plane of ion-saturation data taken at $z=-34$ cm, 4.93 μs after the laser firing. The Langmuir probe is single sided and facing the expanding plasma. It is interesting to note that the extent of the bulk lpp in the $\hat{x}$ direction is approximately twice the directed ion Larmor radius value for doubly ionized Al travelling at 1.4×10^7 cm/s ($R_{Li}=10$ cm) indicating an average charge state of $Z=2$ based purely on radial magnetic confinement. The inset shows the time-evolved trace at $x=-9.5$ cm, $y=-0.5$ cm in the same perpendicular plane. The large initial negative spike is due to escaping fast electrons.[30] The dashed line indicates positions of time-of-flight measurements as discussed next.

An approximation for the total number of lpp ions can be reached by integrating the ion-saturation derived current densities over an entire plane (assuming $Z=2$) and in time. The results obtained in this manner for the total number of ablated particles is consistent with those derived using Faraday cup measurements $N\approx10^{15}$. Since the ion-saturation probe position is known relative to the origin of the laser-produced plasma it can also be used as a time-of-flight (TOF) diagnostic. The relative number of particles passing through a specific x location along the line $y=2.5$ cm, $z=-34$ cm (the dashed line in Fig. 10) with a specific speed normalized to the background ion-sound speed ($c_s=(kT_e/M_i)^{1/2}$) as derived from the TOF is shown in Fig. 10. The speed is considered to be the distance from the origin to the particular position divided by the difference in time between laser firing and time of arrival. While there are some lpp ions travelling above $v_\parallel/c_s=25$, the parallel speed averaged over all x locations is approximately $v_\parallel/c_s=18$, or 0.9×10^7 cm/s as compared to the average initial perpendicular expansion speed of 1.4×10^7 cm/s (note in the background plasma $v_{te}=10^8$ cm/s, $v_{\text{Alfvén}}=5\times10^7$ cm/s, and $c_s=5\times10^5$ cm/s). With an average acoustic Mach number of 18, this supersonic plume should generate acoustic shocks as it moves through the background plasma.

D. Shear Alfvén waves

Whenever time varying current systems with power below f_{ci} are present in a magnetized plasma the possibility for coupling to shear Alfvén waves exists.[31,32] The currents described in this paper vary in time and are expected to radiate shear Alfvén waves. Previously, we reported the generation of shear Alfvén waves from a laser-produced plasma created by a laser incident along the background magnetic field in the original LAPD.[17] The mechanism is essentially the same: the transient lpp currents and the self-consistent currents of the background plasma. Perpendicular expansion adds the asymmetries discussed in Sec. III B which are visible in the early time spatial wave pattern and may draw additional current from the plasma as well as radiate Alfvén waves over a larger volume. The top panel of Fig. 11 shows the fluctuating

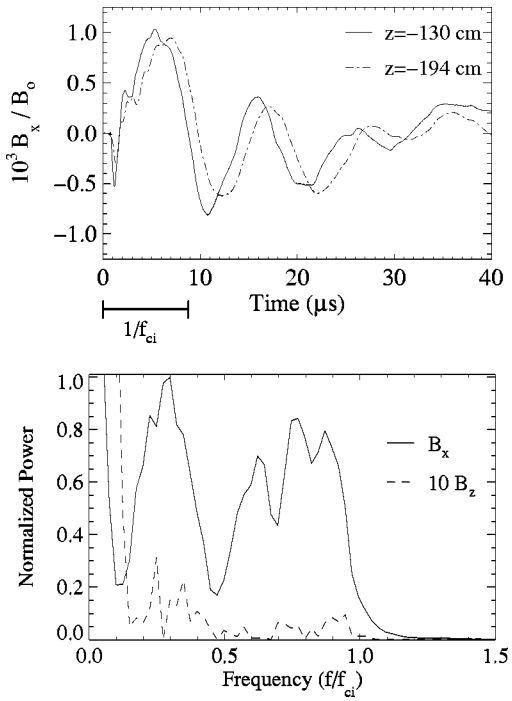

FIG. 11. Top panel, B_x at $x=-10$ cm, $y=-4.5$ cm, $z=-130$, and -194 cm (solid and dashed–dotted, respectively), normalized to background magnetic field, $B_o=1500$ G. $1/f_{ci}$ is shown to indicate mode is below background ion–cyclotron frequency. Bottom panel, power spectrum of B_x and B_z for $z=-194$ cm.

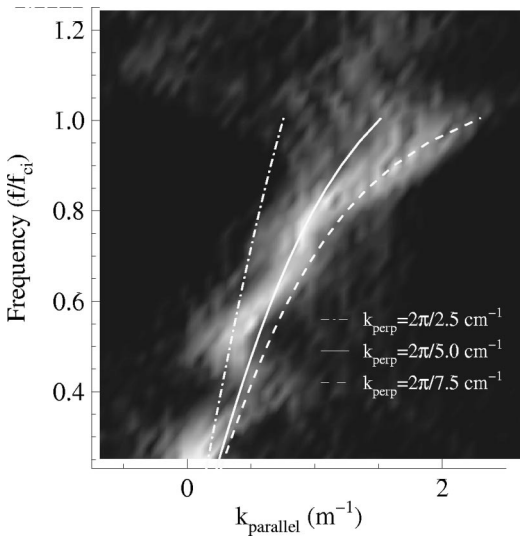

FIG. 12. Frequency and parallel wave number power spectrum. White is highest amplitude. Overplotted lines indicate dispersion relation of kinetic Alfvén waves for a variety of perpendicular wave numbers.

x component of magnetic field at $x=-10$ cm, $y=-4.5$ cm, $z=-130$ cm, and -194 cm (solid and dashed–dotted, respectively). The bottom panel shows the power spectrum of the $z=-194$ cm case as well as that of the corresponding B_z. The power spectrum shows a sharp cutoff at the background ion–cyclotron frequency and very little B_z as one would expect for shear Alfvén waves. Additionally, similar to those observed in previous work, several peaks below the cyclotron frequency can be attributed to standing Alfvén waves on field lines[33] of the 17 m plasma column. The phase delay between the different z locations reveals a propagation speed of $5.6\times10^7\pm0.5$ cm/s consistent with our background Alfvén speed of 5×10^7 cm/s. To positively identify these waves, dispersion relations of the fluctuations were investigated using the statistical method of Beall.[34] Here the local parallel wave number at each frequency is calculated from the phase in the cross-spectrum of two axially separated signals. Typically, this calculation would use two time series that were obtained simultaneously, however, we are relying on the repeatable nature of our experiment and capturing only the waves that are in-phase from shot to shot. To create a large ensemble, measurements from axial pairs (points at the same $x-y$, $z=-34$ cm and $z=-130$ cm) located between -15 cm $<x<0$ cm and -5 cm $<y<5$ cm were used in the average. Using the entire plane gives lower amplitudes since little power is concentrated at the edges. The resulting local parallel wave number ($k_\parallel$) and frequency spectrum is shown in Fig. 12. The overplotted lines correspond to the theoretically predicted dispersion relation for kinetic shear Alfvén waves at a variety of perpendicular wave numbers ($k_\perp$), given below.

$$\omega/k_\parallel=[1-(\omega/\omega_{ci})^2+(k_\perp\rho_s)^2]^{1/2}v_{\text{Alfvén}}, \tag{1}$$

where ρ_s is the ion sound gyroradius: $\rho_s=c_s/\omega_{ci}$.[35,36] The kinetic shear Alfvén wave occurs when the electron thermal speed is greater than the Alfvén speed, namely $v_{te}/v_{\text{Alfvén}}>1$. When $v_{te}/v_{\text{Alfvén}}<1$, the wave is termed an inertial shear Alfvén wave. The properties of these waves have been studied in detail theoretically,[37] as well as experimentally in the LAPD.[31,35,36] To ensure that the waves were propagating throughout analysis, the time series were truncated after the time at which the waves could have interfered and become standing waves. The transition to a standing wave skewed the wave number and frequency spectrum toward $k_\parallel=0$ ($v_{\text{phase}}=\infty$) at the frequencies that turned into standing waves on the field lines, some remnant of which still remains.

Shown in Fig. 13 are magnetic field data on planes perpendicular to B_o taken at $z=-194$ cm, and $t=1.85$ μs and 23.45 μs. At the earlier time, the parallel current sheets are apparent and the pattern is not azimuthally symmetric, rather it is due to a summation of frequencies and perpendicular wave numbers. The later time pattern shows a clear $m=0$ mode structure centered near the location of the initial escaping electron beam current, the dominance of which, over larger perpendicular wave number modes, is due to preferential damping.[33,35,36] The eventual formation of a standing Alfvén wave retains this $m=0$ mode pattern.

The same lines of data used to study the current channel for various values of $v_{te}/v_{\text{Alfvén}}$ in Sec. III A were used to investigate the lpp generation of shear Alfvén wave radiation. Specifically, the amplitude of radiated modes below the background ion–cyclotron frequency for each value of $v_{te}/v_{\text{Alfvén}}$ was calculated. This was accomplished by low pass filtering, below f_{ci}, the received perpendicular

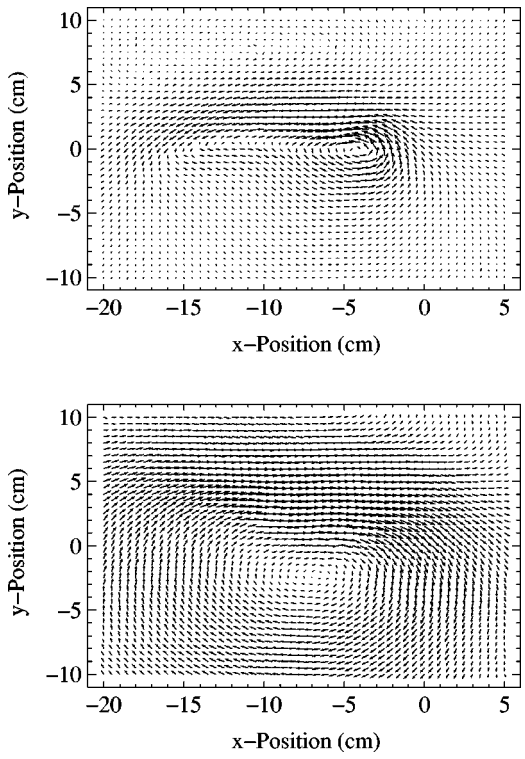

FIG. 13. Planes of perpendicular magnetic field (B_x, B_y) taken at $z=-194$, top/bottom panel $t=1.85$ μs/23.45 μs. Largest vector is 3 G.

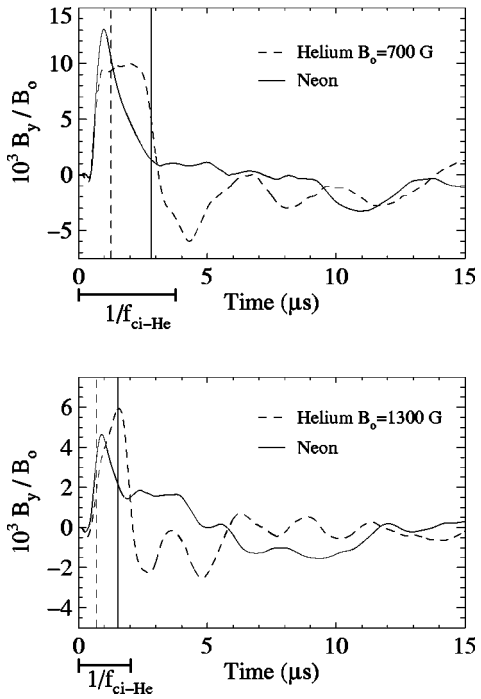

FIG. 15. The y component of wave field ($10^3 B_y/B_o$) measured at $x=-10$ cm, $y=0$ cm, $z=-66$ cm for a carbon target. Results for both neon and helium background plasmas are shown at $B_o=700$ G and 1300 G. $1/f_{ci-\mathrm{He}}$ is shown to indicate oscillations are below the cyclotron frequency. $1/f_{ci-\mathrm{Ne}}$ is $5/f_{ci-\mathrm{He}}$.

magnetic fields at each x location (every 0.5 cm between $x=-15$ cm and 5 cm) along the line $y=0$ cm, $z=-134$ cm and recording the peak amplitude at each location. The resulting peak amplitudes for the various values of $v_{te}/v_{\mathrm{Alfvén}}$ are shown in Fig. 14. $v_{te}/v_{\mathrm{Alfvén}}$ ranges from 2.0 to 0.2, thus going from a regime where the radiated Alfvén waves are kinetic to one where they are inertial. The radiated wave magnitude is observed to go down as $v_{te}/v_{\mathrm{Alfvén}}$ is decreased. This is reasonable since the escaping and return currents having lower magnitudes for lower values of $v_{te}/v_{\mathrm{Alfvén}}$. Meaning that for a given set of lpp conditions it is possible to increase the radiated shear Alfvén wave amplitude simply by increasing the background plasma β. A nonlinear regression fit assuming $B_{\mathrm{wave}}=C_o B_o (v_{te}/v_{\mathrm{Alfvén}})^{C_1}$ for Fig. 14 results in $C_o=3.6\times10^{-3}\pm0.2\times10^{-3}$, $C_1=0.32\pm0.06$. The fit is shown as a solid line in Fig. 14.

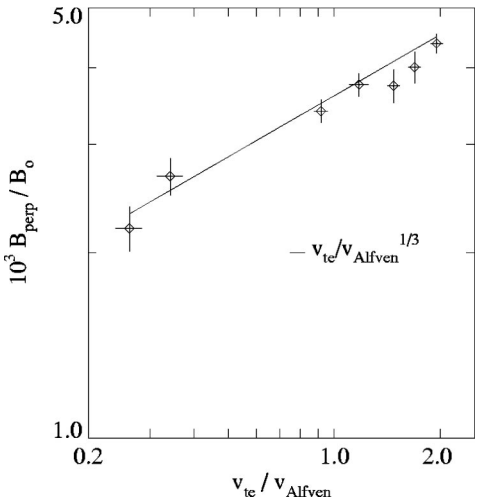

FIG. 14. Peak perpendicular wave field (10^3 $\delta B_{\mathrm{perp}}/B_o$) after low pass filtering (below f_{ci}) vs $v_{te}/v_{\mathrm{Alfvén}}$, $z=-34$ cm. Solid line is nonlinear regression fit.

To further investigate the coupling to shear Alfvén wave radiation the experiment was carried out in a background helium plasma as well as neon plasma ($n_o=2\times10^{12}$ cm^{-3}, $T_e=5$ eV, $T_i=1$ eV) for background magnetic fields of 500, 700, 900, 1100, 1300, and 1500 G. The inductive pickup loop system was placed at $x=-10$ cm, $y=0$ cm, $z=-66$ cm and the y component of the received signals was recorded for 16 μs in helium and 162 μs in neon. The experiment was repeated for 51 shots at each combination of background plasma and magnetic field and the results averaged. The target material for these data was carbon. A carbon target changes the perpendicular and parallel expansion speeds roughly according to the square root of the mass ratio between carbon and aluminum. That is, the perpendicular expansion speed of the carbon lpp is $\approx1.9\times10^7$ cm/s and the parallel expansion speed is $\approx1.2\times10^7$ cm/s.

Shown in Fig. 15 are the received B_y time signals for helium and neon at 700 G and 1300 G. There are some obvious differences as a result of both changing the background magnetic field and plasma ion mass. Considering the 700 G case first, the two vertical lines represent the time delay corresponding to an Alfvén transit time ($T_{\mathrm{Alfvén}}=z/v_{\mathrm{Alfvén}}$) to the probe from the target. In neon, the B_y signal exhibits a quickly rising peak followed by a gradual decay. We attribute this y magnetic field to the outgoing bal-

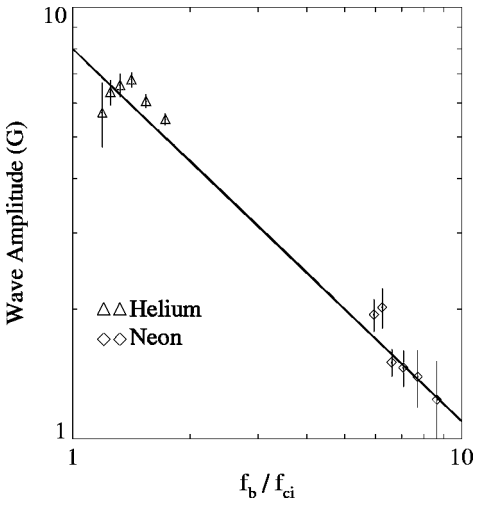

FIG. 16. Wave amplitude obtained by low pass filtering B_y signals below f_{ci} of the background plasma and taking peak amplitude. f_b is $1/4\tau_d$, solid line is to show trend toward increasing wave amplitude as f_b/f_{ci} approaches 1. f_b/f_{ci} was varied by changing background species and magnetic field. B_o values used are 500, 700, 900, 1100, 1300, 1500 G in order of decreasing f_b/f_{ci}.

listic electron current channel. At a much later time ($t > T_{\text{Alfvén}}$), fluctuations arrive which we associate with the shear Alfvén wave radiation. The B_y signal in helium at the same magnetic field is quite different. For helium, due to its lighter mass, the Alfvén speed is greater by a factor of $\sqrt{5}$. Some hint of the original peak as with neon at ≈ 0.9 μs is present, but rather than decay rapidly it sets into oscillation almost directly. Qualitatively, the time signals at 1300 G are the same except that everything happens faster, i.e., the oscillations arrive sooner, consistent with the changing Alfvén speed, the time duration of the impulsive B_y component distinctly observable in the neon series goes down, and the later time oscillations are higher frequency. The FWHM of the first spike in the neon time series actually tracks the diamagnetic cavity lifetime, decreasing as $B^{-2/3}$. The oscillation frequency increases linearly with B, so as to stay below the cyclotron frequency of the background plasma. These findings are significant in that they imply the driver for the shear wave radiation can be tuned with the external magnetic field or target material to couple optimally to the shear wave frequency band ($f < f_{ci}$). Smaller applied magnetic fields increase cavity lifetimes as do heavier target materials due to their slower expansion speeds. The frequency band itself can be adjusted by using different background plasmas. The better coupling is obvious for the helium plasmas where the cyclotron frequency is much closer to that of the cavity lifetime. A dimensionless ratio of relevance to this coupling is therefore

$$f_b/f_{ci} = \frac{\pi}{q}\left(\frac{\pi}{3\mu_o E_{\text{lpp}}}\right)^{1/3}\left(\frac{v_\perp M_i}{B^{1/3}}\right),$$

where $f_b = 1/4\tau_d$. Values of this ratio much larger than one indicate that the original ballistic electron current channel will have very little power below the background cyclotron frequency and consequently possibly couple poorly to shear Alfvén waves.

Since this series of experiments was carried out for laser incidence perpendicular to the confining magnetic field, the current channel was swept across the background plasma creating current sheets as mentioned in Sec. III B. This launches a broad range of perpendicular wave numbers and adds additional timescales. For incidence along the confining field, it is not expected that these sheets will form and a greater control over the perpendicular wave numbers can be exercised simply by adjusting the background field.

Figure 16 shows the peak amplitude of the low pass filtered ($f < f_{ci}$) signals for various values of f_b/f_{ci}. The peak wave amplitudes in helium are a factor of 3–4 larger than in neon. The helium wave amplitudes reach a peak value of approximately 6 G and do not continue to grow as f_b/f_{ci} is lowered. This may be due to limitations placed by the background thermal current or simply the fact that all measurements were made at the same location. As the background field is increased, it is expected that the wave fields will become localized over a smaller region, a fact which cannot be taken into account without further measurements.

Since a semivolumetric data set was taken with a neon background plasma, an approximation can be arrived at for the total energy contained in fluctuating magnetic fields. If only fluctuations on the shear Alfvén branch are considered ($f < f_{ci}$), one arrives at $E_{\text{shear}} \approx 0.01 E_{\text{lpp}}$. This is very similar to the previously determined value for laser incidence coincident with the background magnetic field.[17] Based on the measured wave fields presented in Fig. 16, however, it is possible that by tuning the ratio of f_b/f_{ci} the fraction of lpp kinetic energy converted to shear Alfvén wave energy could be made larger by a factor of approximately 10 or more.

IV. SUMMARY AND DISCUSSION

The expansion of a laser-produced plasma from a flat surface ($R_{\text{laser-beam}} \ll R_{\text{target}}$), generated by irradiation perpendicular to a confining magnetic field, into an ambient magnetized background plasma has been studied. The lpp is observed to travel across the background magnetic field while simultaneously undergoing electric polarization and generating current structures in the background plasma. Later expansion is primarily directed along the field with little radial lpp loss. The background plasma responds by generating a variety of waves, the dominant magnetic response is due to shear Alfvén wave radiation. One percent of the expanding lpp kinetic energy is radiated into these waves. The current responsible for driving the shear Alfvén waves arises from escaping lpp electrons and has a lifetime similar to that of the diamagnetic cavity lifetime. The peak current densities are found to scale as $J_{te}(v_{te}/v_{\text{Alfvén}})^{-2/3}$ while the peak wave fields scale as $v_{te}/v_{\text{Alfvén}}{}^{1/3}$, predicting a common temperature dependence of $T_e^{1/6}$, but a differing density dependence, $n^{2/3}$ and $n^{1/6}$ for the current densities and wave fields, respectively. One may expect the current densities and wave fields to scale in the same manner. This may be the case, however, since we only varied density by a factor of 2.6 the disagree-

ment is not obvious. The parallel current driver can be made to deposit more power into Alfvén waves based on the ratio f_b/f_{ci}. Additionally, it is possible to increase the driven current densities and consequently wave amplitudes by increasing the background $v_{te}/v_{\text{Alfvén}}$. Other effects such as drift waves, beam-plasma instabilities, compressional Alfvén waves, and acoustic waves will be the subject of future research.

These results may be applicable to a variety of situations where expanding plasmas are present in an ambient background plasma. For example, in tokamak fuelling, it has been hypothesized[38] that there is an induced polarization from high-field side injected pellets due to magnetic curvature and $\vec{\nabla}\vec{B}$ charged particle drifts. This polarization can then drive parallel current flows and the emission of Alfvén waves.[28,29,39] On the surface of the sun, mass ejections may create currents in the ambient corona and consequently radiate Alfvén waves in an analogous manner. In the STARFISH situation undoubtedly fast particles created parallel current flows in the ionosphere which closed through the expanding plasma creating Alfvén waves. Another application of this research may be in the slowing of expanding plasmas by Alfvén wave radiation and $\vec{J}\times\vec{B}$ forces on the generated current structures.[28,40]

ACKNOWLEDGMENTS

We are indebted to Professor G. Morales for many insightful discussions as well as F. Tsung for explanations and comparisons to their simulation. Additionally, the authors wish to thank G. Dimonte for his help with the preliminary experiments and also the discussion of his own laser-plasma experiments and simulation results. We also acknowledge the advice of G. Dipeso and D. Hewett and thank them for sharing their simulation results with us. Also, we are grateful to M. Drandell for his expert technical assistance.

This work was funded by the Department of Energy Contract No. DE-F603-98ER54494 and the Office of Naval Research (N00014-97-1-0167). M.V.Z.'s research was performed under appointment to the Fusion Energy Sciences Fellowship Program administered by Oak Ridge Institute for Science and Education under a contract between the U.S. Department of Energy and the Oak Ridge Associated Universities.

[1] J. Gosling, Phys. Fluids B **5**, 2638 (1993).
[2] M. Neugebauer, R. Goldstein, and B. Goldstein, J. Geophys. Res. **102**, 19743 (1997).
[3] P. Taylor, A. Kellman, A. T. Evans *et al.*, Phys. Plasmas **6**, 1872 (1999).
[4] H. Strauss and W. Park, Phys. Plasmas **7**, 250 (2000).
[5] Series of articles on *starfish*, J. Geophys. Res. **68** (1963).
[6] P. Bernhardt, Phys. Fluids B **4**, 2249 (1992).
[7] D. Gurnett, R. Anderson, T. Ma *et al.*, J. Geophys. Res. **91**, 10013 (1986).
[8] J. M. Dawson, Phys. Fluids **7**, 981 (1964).
[9] A. Glass, J. Vac. Sci. Technol. A **4**, 1098 (1986).
[10] S. Bodner, D. Colombant, J. Gardner *et al.*, Phys. Plasmas **5**, 1901 (1998).
[11] R. Peterson, D. Haynes, I. Golovkin, and G. Moses, Phys. Plasmas **9**, 2287 (2002).
[12] V. Antonov, V. Bashurin, A. Golubev *et al.*, J. Appl. Mech. Tech. Phys. **26**, 757 (1985).
[13] B. A. Remington, R. P. Drake, H. Takabe, and D. Arnett, Phys. Plasmas **7**, 1641 (2000).
[14] R. K. Singh and J. Narayan, Phys. Rev. B **41**, 8843 (1990).
[15] W. Gekelman, H. Pfister, Z. Lucky, J. Bamber, D. Leneman, and J. Maggs, Rev. Sci. Instrum. **62**, 2875 (1991).
[16] L. Mandrake and W. Gekelman, Comput. Phys. **11**, 498 (1997).
[17] M. VanZeeland, W. Gekelman, S. Vincena, and G. Dimonte, Phys. Rev. Lett. **87**, 105001 (2001).
[18] G. Dimonte, G. Dipeso, and D. Hewett (private communication).
[19] G. Dimonte and L. Wiley, Phys. Rev. Lett. **67**, 1755 (1991).
[20] S. Kacenjar, M. Hausman, M. Keskinen *et al.*, Phys. Fluids **29**, 2007 (1986).
[21] B. Ripin, J. Huba, E. Mclean *et al.*, Phys. Fluids B **5**, 3491 (1993).
[22] J. Grun, R. Decoste, B. Ripin, and J. Gardner, Appl. Phys. Lett. **39**, 545 (1981).
[23] B. Meyer and G. Thiell, Phys. Fluids **27**, 302 (1984).
[24] B. Ripin, R. Whitlock, F. Young, S. Obenschain, E. McLean, and R. Decoste, Phys. Rev. Lett. **43**, 350 (1979).
[25] B. Ripin, E. McLean, C. Manka *et al.*, Phys. Rev. Lett. **59**, 2299 (1987).
[26] F. Tsung, G. Morales, and J. Leboeuf, Phys. Rev. Lett. **90**, 055004 (2003).
[27] A. Mostovych, B. Ripin, and J. Stamper, Phys. Rev. Lett. **62**, 2837 (1989).
[28] J. E. Borovsky, Phys. Fluids **30**, 2518 (1987).
[29] M. Galvez and J. Borovsky, Phys. Fluids B **3**, 1892 (1991).
[30] R. Issac, P. Gopinath, G. Varier, V. Nampoori, and C. Vallabhan, Appl. Phys. Lett. **73**, 163 (1998).
[31] W. Gekelman, D. Leneman, J. Maggs, and S. Vincena, Phys. Plasmas **1**, 3775 (1994).
[32] S. T. Vincena and W. N. Gekelman, IEEE Trans. Plasma Sci. **27**, 144 (1999).
[33] C. Mitchell, S. Vincena, J. Maggs, and W. Gekelman, Geophys. Res. Lett. **28**, 923 (2001).
[34] J. M. Beall, Y. C. Kim, and E. J. Powers, J. Appl. Phys. **53**, 3933 (1982).
[35] S. Vincena, W. Gekelman, and J. Maggs, Phys. Plasmas **8**, 3884 (2001).
[36] S. Vincena, Ph.D. thesis, University of California at Los Angeles, 1999.
[37] G. J. Morales and J. E. Maggs, Phys. Plasmas **4**, 4118 (1997).
[38] P. Parks, W. Sessions, and L. Baylor, Phys. Plasmas **7**, 1968 (2000).
[39] L. L. Lengyel, IEEE Trans. Plasma Sci. **20**, 663 (1992).
[40] S. Drell, H. Foley, and M. Ruderman, J. Geophys. Res. **70**, 3131 (1965).